Stromal Expression of Activated Leukocyte Cell Adhesion Molecule Promotes Lung Tumor Growth and Metastasis

Willrodt, Ann-Helen ; Beffinger, Michal ; Vranova, Martina ; Protsyuk, Darya ; Schuler, Katja ; Jadhav, Maria ; Heikenwalder, Mathias ; van den Broek, Maries ; Borsig, Lubor ; Halin, Cornelia

Abstract: Activated leukocyte cell adhesion molecule (ALCAM) is expressed on various cell types, including leukocytes, endothelial cells, and certain tumor cells. Although ALCAM expression on tumor cells has been linked to tumor invasion and metastatic spread, the contribution of ALCAM expressed in cells forming the tumor stroma to cancer progression has not been investigated. In this study, ALCAM-deficient (ALCAM-/-) mice were used to evaluate the role of ALCAM in lung tumor growth and metastasis. ALCAM-/- mice displayed an altered blood vascular network in the lung and the diaphragm, indicative of an angiogenetic defect. The absence of ALCAM expression in cells forming the stromal tumor microenvironment profoundly affected lung tumor growth in three different i.v. metastasis models. In the case of Lewis lung carcinoma (LLC), an additional defect in tumor cell homing to the lungs and a resulting reduction in the number of lung tumor nodules were observed. Similarly, when LLC cells were implanted subcutaneously for the study of spontaneous tumor cell metastasis, the rate of LLC metastasis to the lungs was profoundly reduced in ALCAM-/- mice. Taken together, our work demonstrates for the first time the in vivo contribution of ALCAM to angiogenesis and reveals a novel role of stromally expressed ALCAM in supporting tumor growth and metastatic spread.

DOI: https://doi.org/10.1016/j.ajpath.2017.07.008

Regular Article:

Stromal expression of activated leukocyte cell adhesion molecule (ALCAM) promotes lung tumor growth and metastasis

Ann-Helen Willrodt[1], Michal Beffinger[2*], Martina Vranova[1*], Darya Protsyuk[3], Katja Schuler[1], Maria Jadhav, Mathias Heikenwalder[4], Maries van den Broek[2], Lubor Borsig[3], Cornelia Halin Winter[1]

[1]Institute of Pharmaceutical Sciences, ETH Zurich, Switzerland

[2]Institute of Experimental Immunology, UZH Zurich, Switzerland

[3]Institute of Physiology, UZH Zurich, Switzerland

[4]Division of Chronic Inflammation and Cancer, German Cancer Research Center (DKFZ), Heidelberg, Germany

* these authors contributed equally to this work

Corresponding author:

Cornelia Halin, Ph.D.

Institute of Pharmaceutical Sciences, ETH Zurich

Wolfgang-Pauli Str. 10,

CH-8093 Zurich, Switzerland

e-mail: cornelia.halin@pharma.ethz.ch

Phone: +41 44 633 29 62

Running title: Stromal ALCAM supports lung metastasis

Financial support was received from the Swiss National Science Foundation (310030_138330), the Promedica Foundation and ETH Zurich (all to CH).

Disclosures: None declared.

Abstract

Activated leukocyte cell adhesion molecule (ALCAM) is expressed on various cell types, including leukocytes, endothelial cells and certain tumor cells. While ALCAM expression in tumor cells has been linked with tumor invasion and metastatic spread, the contribution of ALCAM expressed in cells forming the tumor stroma to cancer progression has not been investigated. In this study, we made use of ALCAM-deficient ($ALCAM^{-/-}$) mice to evaluate the role of ALCAM in lung tumor growth and metastasis. $ALCAM^{-/-}$ mice displayed an altered blood vascular network in the lung and the diaphragm, indicative of an angiogenesis defect. Absence of ALCAM expression by cells forming the stromal tumor microenvironment profoundly impacted lung tumor growth in three different intravenous metastasis models. In the case of Lewis lung carcinoma (LLC), an additional defect in tumor cell homing to the lungs and a resulting reduction in the number of lung tumor nodules was observed. Similarly, when LLC were subcutaneously implanted to study spontaneous tumor cell metastasis, the rate of LLC metastases to the lungs was profoundly reduced in $ALCAM^{-/-}$ mice. Taken together, our work demonstrates for the first time the *in vivo* contribution of ALCAM to angiogenesis and reveals a novel role of stromally expressed ALCAM in supporting tumor growth and metastatic spread.

Introduction

Cell adhesion molecules (CAMs) are transmembrane proteins, which are involved in cell-cell and cell-extracellular matrix (ECM) interactions. Many studies have documented the involvement of CAMs in various steps of tumor progression and metastatic spread, namely in tumor cell interaction with the ECM, invasion, expansion of the intra- and peritumoral vasculature, entry and exit of tumor cells from the circulation and finally metastatic outgrowth in distant organs [1, 2]. In addition, CAMs are crucial for the recruitment and activation of leukocytes during an anti-tumor immune response [3]. Activated leukocyte cell adhesion molecule (ALCAM, CD166) is a member of the immunoglobulin superfamily and has been implicated in many of the above-mentioned processes. ALCAM engages in homophilic, as well as heterophilic interactions with its binding partners CD6, galectin 8 and L1CAM [4-6]. ALCAM expression by T cells [7] and monocytes [8] was shown to mediate the migration of leukocytes across ALCAM-expressing endothelial cell monolayers, whereas the interaction of ALCAM expressed on dendritic cells with CD6 expressed on T cells reportedly contributes to T cell activation *in vitro* [9, 10]. In addition, ALCAM expressed by vascular endothelial cells was shown to support angiogenic processes *in vitro* [11, 12]. Although the expression of ALCAM in blood vessels *in vivo* has been demonstrated in the human and murine central nervous system (CNS) [7, 13], the human skin [11], the rat lung [14] and the murine liver and lung [11, 15], its *in vivo* contribution to angiogenesis has not been investigated to date. In this context, our group has recently described the expression of ALCAM in lymphatic endothelial cells and its involvement in the formation of lymphatic vessels, thereby providing the first *in vivo* evidence of the relevance of ALCAM for endothelial cell biology [11]. Moreover, a recent study has reported the role of ALCAM in regulating the expression of tight junction proteins and controlling vascular permeability of the blood brain barrier [13].

In addition to leukocytes and endothelial cells, several other cells such as neurons [16], certain epithelial cells [17] and keratinocytes [18] reportedly express ALCAM. Moreover, ALCAM expression by cancer cells has been linked with the grade of tumor malignancy, apoptotic resistance, epithelial-mesenchymal transition and patient prognosis [3]. For example, in gastric cancer [19], colorectal cancer [20, 21], pancreatic cancer[22], prostate cancer [23, 24], or melanoma [25-27] ALCAM

expression was shown to positively correlate with cancer progression. The tumor stroma, which consists of cells forming the tumor vasculature, immune cells, fibroblast and the ECM, is known to directly impact tumor cell survival, tumor growth and progression [28-30]. However, up to now the contribution of stromal ALCAM to *in vivo* tumor growth has not been examined. In this study, we investigated lung tumor growth and metastatic spread in ALCAM$^{-/-}$ compared to wild-type (WT) mice. Performing experiments in three different intravenous lung metastasis models we show that absence of ALCAM expression in stromal cells markedly reduced metastatic outgrowth in the lungs of ALCAM$^{-/-}$ compared to WT mice. The tumor growth retardation was associated with an angiogenesis defect and – in the case of LLC – with reduced ability of tumor cells to home to the lungs of ALCAM$^{-/-}$ mice. In sum, our work reveals a novel contribution of ALCAM expressed by cells forming the stromal tumor microenvironment to metastatic spread and tumor outgrowth in the lung.

Materials and Methods

Mice

WT C57BL/6-J mice (Janvier, Genest-Saint-Isle, France) and ALCAM$^{-/-}$ mice [16] obtained from Jackson Laboratories (Bar Harbor, ME, USA) were housed in the animal facility of ETH Zurich or of the University of Zurich. All experiments were approved by the Cantonal Veterinary Office Zurich.

Cell lines

The melanoma cell line B16F10 cell line (B16F10; Caliper, Hopkinton, MA, USA) transfected with luciferase (B16F10-luc2) was kindly provided by Dr. Michael Detmar, ETH Zurich. Cells were cultured in DMEM (Invitrogen, Carlsbad, CA, USA) supplemented with 10 % FCS (Life

Technologies, Carlsbad, CA, USA) and 1 % antibiotic-antimycotic (Life Technologies). The colon adenocarcinoma cell line MC38 GFP [31], the LLC cell line [32] (from ATCC) as well as LLCs lentivirally transfected with luciferase were cultured as previously described [33]. Human umbilical vein endothelial cells (HUVECs; Promocell, Heidelberg, Germany) were cultured on plates coated with 10 μg/ml collagen type I (Advanced BioMatrix, Poway, CA, USA) and 10 μg/ml fibronectin (Merck Millipore, Darmstadt, Germany) in EGM-2MV medium without VEGF-A (Lonza, Basel, Switzerland). Mouse Mile Sven-1 (MS-1) cells [34] were cultured in DMEM (Sigma-Aldrich, St. Louis, MO, USA) supplemented with 5 % FCS (Life Technologies) and 1 % antibiotic-antimycotic (Life Technologies).

Scratch-wound assay

Confluent HUVEC and MS-1 monolayers grown in 24-well plates were cultured for 24 hours in starvation medium containing FCS (Life Technologies; HUVEC: 2%; MS-1: 5%) and 1 % antibiotic-antimycotic solution (Life Technologies). Assays were performed as described in [11], using anti-human ALCAM (R&D Systems, Abingdon, UK) or goat IgG (all at 10 μ g/ml) in starvation medium. For HUVECs assays were performed in presence of human VEGF-A (20 ng/ml; PeproTech, London, UK) in starvation medium.

Immunohistology of murine tissues

Immunohistology of murine diaphragms was performed as previously described [11]. In brief, diaphragm whole mounts were blocked in 1 % BSA, 0.05 % sodium azide, 0.01 % Triton-x and 5% normal donkey serum (Sigma-Aldrich) in PBS for 1 h and stained with rat anti-mouse CD31 (BD Bioscience, Franklin Lakes, NJ, USA) in PBS overnight. The next day, diaphragms were washed and incubated for 2 hours with anti-rat AlexaFlour 488-conjugated secondary antibody (Invitrogen). Images were acquired on a LSM 710 FCS confocal microscope (Carl Zeiss Inc., Jena, Germany) using 10x objective (NA of 0.3) and analyzed with ImageJ software. To

125 exclusively analyze blood vessels, $CD31^+$ lymphatic vessels (identified by their $CD31^{dim}$ staining
126 and large vessel diameter) were removed from the image prior to analysis.
127 For immunohistological analysis of mouse lungs, mice were euthanized and perfused with PBS
128 followed by a 4 % PFA solution for fixation. After 2 days in 4 % PFA, lungs were embedded in
129 paraffin. In the case of α-smooth muscle actin (αSMA) staining, lung sections (6 μm) were stained
130 on a staining robot (BondMax, Leica Microsystems, Wetzlar, Germany) with anti-mouse αSMA
131 antibody (Sigma-Aldrich), followed by incubation with secondary rabbit anti-mouse-IgG (Abcam,
132 Cambridge, UK). Final detection of bound antibody was performed using the Bond Polymer
133 Refine detection DAB-Kit (Leica Microsystems). For the vWF staining, lung sections were
134 incubated at 60 °C for 10 min, followed by deparaffinization and rehydration. Sections were
135 incubated for 1 hour at room temperature in blocking solution (3 % BSA, 0.1 % NP40 (both from
136 Sigma-Aldrich) in PBS). Subsequently, rabbit anti-mouse vWF (Dako, Glostrup, Denmark) in
137 blocking solution was added overnight at 4 °C. The next day, sections were washed and anti-
138 rabbit AlexaFluor 594 (Invitrogen) was applied for 1 hour at room temperature in PBS. Sections
139 were mounted using Mowiol (Calbiochem, San Diego, CA, USA). For the quantification of the
140 vWF^+ or αSMA^+ vessel area, five (vWF) or nine (αSMA) images per lung were acquired. Vessels
141 that were completely visible within the field of view were encircled using Adobe Photoshop CS5
142 (Adobe System, San Jose, CA), followed by quantification of the vessel area and vessel number.
143 For the analysis of MC38 tumor vascularization and vessel maturation, OCT-embedded, frozen
144 sections (6 μm) were fixed in acetone (2 min at -20 °C) and methanol (5 min at 4 °C) followed by
145 two washing steps in Tris-buffered saline (TBS). Sections ware stained with rat anti-mouse CD31
146 (clone MEC13.3, BD Pharmingen, San Jose, CA, USA) and rabbit anti-mouse NG2 (polyclonal
147 antibody, Merck) in antibody diluent (Zytomed Systems, Berlin, Germany) overnight at 4 °C. After
148 washing with TBS, AlexaFluor 488- and 594-coupled secondary antibodies (Invitrogen) were
149 added for detection. Sections were mounted using Mowiol (Calbiochem). For quantification of
150 $CD31^+$ and $CD31^+$ $NG2^+$ vessels, images of three vascularized areas per tumor nodule were
151 acquired (as described below) and analyzed using ImageJ. The area of $CD31^+$ vessels was

152 determined after tresholding. Subsequently the percentage of vessels that were $NG2^+$ among
153 $CD31^+$ vessels was determined.
154 For the analysis of macrophage infiltration into MC38 tumor nodules, OCT-embedded, frozen
155 sections (6 μm) were fixed in acetone (2 min at -20 °C) and methanol (5 min at 4 °C) followed by
156 two washing steps in PBS. Sections were incubated for 45 minutes at room temperature in
157 blocking solution (2 % BSA, 5 % normal donkey serum (NDS), 0.1% TritonX (all from Sigma-
158 Aldrich) in PBS). Subsequently, rat anti-mouse F4/80 (clone BM8, eBioscience, San Diego, CA,
159 USA) and goat anti-mouse CD206 (polyclonal antibody, R&D) in PBS with 5% NDS were added
160 overnight at 4 °C. After washing with PBS, AlexaFluor 488- and 594-coupled secondary
161 antibodies (Invitrogen) were added for detection. Sections were mounted using Mowiol
162 (Calbiochem). For quantification of $F4/80^+$ and $F4/80^+$ $CD206^+$ cells, three images per tumor
163 nodule were acquired (as described below) and analyzed using ImageJ.
164 For the quantification of tumor nodule area, frozen MC38 sections were stained with
165 haemotoxylin/eosin (H&E) and stitched images of the entire tumor nodule were acquired and
166 analyzed using Adobe Photoshop CS5 (Adobe System). Images were acquired with an Axioskop
167 2 MOT plus microscope (Carl Zeiss Inc.) using the following objectives: 10 x objective, NA of 0.3
168 (for lung sections stained for vWF and αSMA); 20 x objective, NA of 0.5 (for MC38 lung tumor
169 sections stained for CD31/NG2 and F4/80/CD206); and 5 x objective; NA of 0.15 (H&E stainings).
170 The microscope was equipped with an AxioCam MRm monochrome digital camera (Carl Zeiss
171 Inc.) and AxioVision 4.4 software (Carl Zeiss Inc.).
172

173 **Immunohistology of human tissues**

174 6 μm sections of human foreskin and human lungs (Zyagen, USA) were analyzed for ALCAM
175 expression. After fixation with acetone (2 minutes at -20 °C) and 80% methanol (5 minutes at
176 4°C), sections were stained with mouse anti-human CD31 (Dako, clone JC70A) or mouse anti-
177 human αSMA–Cy3 (Sigma, clone 1A4) and goat anti-mouse ALCAM (R&D, polyclonal antibody)
178 or corresponding goat isotype control (Invitrogen) overnight at 4°C in a PBS blocking solution

containing 2% BSA, 5% normal donkey serum and 0.1% tween (all from Sigma-Aldrich). After washing, anti-mouse Alexa Fluor 594 and anti-goat Alexa Fluor 647 (Invitrogen) were added for 1 hour at room temperature. Confocal images were acquired at a LEICA TCS SP8 microscope using a 20x objective (NA of 0.7, Leica).

FACS analysis

FACS analysis of *in vitro*-cultured cells and tissues was performed as previously described [11]. In brief, *in vitro*-cultured cells were washed with PBS and detached using accutase (Sigma-Aldrich). For tissue FACS, tissues were digested in PBS supplemented with 4 mg/ml collagenase IV (Gibco) for 1h at 37°C. In the case of lungs, collagenase IV was resuspended in Grey's Balanced Salt Solution (GBSS, Sigma-Aldrich). Cell suspensions were stained with anti-mouse CD31-APC, anti-mouse CD45-PerCP, CD45-APC and podoplanin-PE and corresponding isotype controls (all from Biolegend, San Diego, California, USA). Dead cells were excluded using Zombie dye (Biolegend). ALCAM expression was detected by staining with goat anti-mouse ALCAM antibody and corresponding AlexaFluor488- or PE-labeled secondary antibodies (Invitrogen). Data were acquired on a BD FACSCanto (BD Bioscience, Franklin Lake, NJ, USA) using FACSDiva software (BD Bioscience) and analyzed with FlowJo software 8.7.1. (Treestar, Ashland, TN, USA).

Homing studies

12-15 week old WT or ALCAM$^{-/-}$ mice were used for homing studies. Prior to tumor cell injection, tumor cells (LLC or B16F10) were stained with 5 mM CFSE (Invitrogen) for 15 min at 37°C in PBS, followed by neutralization of unused dye with equal volumes of media. After washing cells twice with PBS, mice were injected with 1x10^6 cells i.v.. 24 hours later, mice were sacrificed, perfused with PBS and the lungs were harvested. Lungs were cut in small pieces and digested for 45 min at 37°C in 4 mg/ml collagenase IV (Gibco) in PBS. Subsequently, the lungs were passed through a 40 μm cell strainer and subjected to red blood cell lysis using ACK buffer. Lung

206 single cell suspensions were stained with CD45-APC (Biolegend). $CD45^-$ $CFSE^+$ tumor cells were
207 quantified by FACS with the help of counting beads (Invitrogen).

208

209 **Tumor models**

210 12-15 week old WT or $ALCAM^{-/-}$ mice were used for tumor studies. For the lung metastasis model
211 mice were injected i.v. with tumor cells (B16F10-Luc: $1x10^6$; LLC: $1.5x10^5$; MC38-GFP $3x10^5$).
212 After 12-26 days (B16F10 and LLC: 12-14 days; MC38: 26 days) mice were sacrificed and the
213 tumor burden was analyzed. B16F10 tumor growth was monitored *in vivo* by intraperitoneal (i.p.)
214 injection of 150 mg luciferin/kg body weight and imaging the luminescent signal in the thorax 20
215 min later with an IVIS Spectrum imaging system (Caliper) under isoflurane anesthesia. At the end
216 of the experiment, mice were sacrificed and the luciferase signal was measured in excised lungs
217 and in lung single cell suspensions (see below). For the spontaneous lung metastasis model,
218 mice were injected s.c. with $0.2x10^6$ LLC cells. Primary tumors were resected after 21 or 24 days.
219 The metastatic burden was quantified three weeks later using an IVIS Spectrum imaging system
220 (Caliper), as mentioned above.

221

222 ***In vitro* luciferase activity assay**

223 Lung tissue was homogenized in lysis buffer containing 25 mM Tris - Cl pH 7.8 (Fluka), 2 mM
224 EDTA (Sigma-Aldrich), 1 mM dithiothreitol (DTT, Promega, Madison, WI, USA), 10 % glycerol
225 (ABCR, Karlsruhe, Germany), 1 % Triton X-100 (Fluka) and one Complete Mini, EDTA - free
226 Protease Inhibitor Tablet (Roche, Basel, Switzerland) (1 tablet was added to 10 ml of lysis
227 buffer). Samples were homogenized using a TissueLyser (Qiagen, Venlo Netherlands; Retsch,
228 Haan, Germany) followed by centrifugation. Luciferase activity was measured with an IVIS
229 Spectrum (Caliper) using 25 µl tissue lysate and 50 µl assay buffer, which consisted of 20 mM
230 Tris - Cl (Fluka), 1.1 mM MgCl (Fluka), 2.7 mM $MgSO_4$ x $7H_2O$ (Fluka), 0.1 mM EDTA, 33.3 mM
231 DTT (Promega, Madison, WI, USA), 530 µM ATP (Sigma-Aldrich) and 400 µM luciferin (Caliper).

Statistical data analysis

Statistical analysis was performed using Prism 6 (GraphPad Software, La Jolla, CA, USA). Normally distributed data was analyzed using the student's *t*-test or one-way ANOVA (more than two groups) and are presented as mean ± standard error (SEM). To test for significant differences in the rate of metastases a chi-squared test was applied. Significant outliers were identified based on Grubbs test and excluded. Differences were considered statistically significant when $p < 0.05$.

Results

ALCAM is expressed in the human and murine vasculature and contributes to *in vitro* angiogenesis

We have recently described an *in vivo* role for ALCAM in the formation of the lymphatic network in mice [11]. Moreover, several studies have previously reported on the expression of ALCAM in blood vessels [7, 11, 14, 15] and on its involvement in endothelial cell biology *in vitro* [11, 12]. In agreement with previous findings [11], we detected ALCAM expression in the vasculature of human skin (Fig. 1A). Moreover, we identified ALCAM-positive blood vessels in tissue sections of human lung (Fig. 1B). High magnification confocal images of the vasculature in the human lung revealed that ALCAM was primarily expressed in endothelial cells but not in vessel-surrounding mural cells (Fig. S1A,B). Interestingly, in the mouse, FACS analysis performed on tissue single cell suspensions revealed ALCAM expression in endothelial cells derived from the murine lung (Fig. 1C), but not from murine skin (Fig. 1D). Moreover, ALCAM was also expressed by non-endothelial stromal cells (i.e. fractions of $CD31^-CD45^-podoplanin^+$ and $CD31^-CD45^-podoplanin^-$ cells; Fig. S1C,D). We next performed *in vitro* endothelial cell migration assays with ALCAM-expressing human umbilical vein endothelial cells (HUVECs) and the immortalized murine blood vascular endothelial cell line MS-1 [34] (Fig. 1E,F). In both cell types, the ability of the endothelial cells to migrate into a cell-free area was significantly reduced in presence of an ALCAM blocking antibody (Fig. 1G,H), confirming that ALCAM supports angiogenic processes *in vitro.*

ALCAM contributes to angiogenesis *in vivo*

To investigate whether ALCAM contributes to angiogenesis *in vivo,* we analyzed the blood vasculature in the lung and the diaphragm of $ALCAM^{-/-}$ mice [16]. Performing whole mount analyses in the diaphragm of pups we found that the total area covered by $CD31^+$ blood vessels as well as the average blood vessel diameter were markedly reduced in $ALCAM^{-/-}$ compared to WT diaphragms (Fig. 2A-C). Moreover, when staining murine lung sections for the blood vascular marker von Willebrand Factor (vWF; Fig. 2D) we observed that the size of vWF^+ vessels was

profoundly reduced in ALCAM$^{-/-}$ compared to WT mice (Fig. 2E). By contrast, when staining murine lung sections with the pericyte marker alpha smooth muscle actin (αSMA; Fig. 2F), no difference in the size of αSMA^{+} vessels, which typically represent the larger vessels, was observed (Fig. 2G). However, the total number of αSMA^{+} vessels (Fig. 2H) was significantly reduced. Taken together, these results revealed an angiogenesis defect in the lung and the diaphragm and suggested general alterations in the blood vasculature of ALCAM$^{-/-}$ mice.

Growth of B16F10 lung metastases is reduced in ALCAM$^{-/-}$ mice

Given the expression of ALCAM on human and murine blood vessels in the lung (Fig. 1B,C) and its impact on *in vivo* angiogenesis (Fig. 2 D-H), we next investigated tumor growth in this organ. To this end, mice were injected intravenously (i.v.) with a luciferase-expressing B16F10 melanoma cell line. When subsequently monitoring luciferase activity over 12 days by IVIS we found that luciferase signals were consistently lower in ALCAM$^{-/-}$ compared to WT mice (Fig. 3A/B). The reduced metastatic burden in ALCAM$^{-/-}$ compared to WT mice was confirmed at the end of the study, by measuring the luciferase activity in excised lungs (Fig. 3C) or in lung homogenates (Fig. 3D). No significant differences were found when quantifying visible lung metastases in WT and ALCAM$^{-/-}$ mice (Fig. 3E), or when performing tumor cell homing studies (Fig. S2), suggesting that the loss of stromal ALCAM expression did not affect the ability of ALCAM-expressing B16F10 cells (Fig. 3F) to home and seed to the lung. By contrast, the overall area covered by visible metastases was profoundly reduced in ALCAM$^{-/-}$ mice (Fig. 3G). Moreover, when analyzing the size distribution of metastases in both genotypes, we observed that ALCAM$^{-/-}$ mice had almost no large metastases (defined as metastases with a diameter of > 350 μm), but an increased number of small metastases (diameter < 200 μm) (Fig. 3H). Taken together, these findings suggested a growth disadvantage of B16F10 metastases in the lungs of ALCAM$^{-/-}$ mice.

Stromal ALCAM deficiency reduces MC38 tumor growth and angiogenesis

We next performed similar experiments with MC38 adenocarcinoma cells (Fig. 4A), which form fewer but larger tumor nodules in the lungs upon i.v. injection (Fig. 4B). When dissecting the lungs 24-28 days after tumor cell injection, no difference in tumor nodule numbers was observed between the genotypes (Fig. 4C). However, the average lung tumor nodule weight was profoundly reduced in ALCAM$^{-/-}$ mice (Fig. 4D), confirming the metastatic growth defect previously observed in the B16F10 model. In line with the reduced tumor weight, H&E staining revealed that also the average tumor area (Fig. 4E) and the overall percentage of large tumors (Fig. 4F,G) was reduced in ALCAM$^{-/-}$ compared to WT mice. To investigate whether the reduction in tumor size was caused by a defect in angiogenesis, we analyzed tumor vascularization by immunofluorescence. No Lyve-1^{+} lymphatic vessels could be detected within the tumor nodules (data not shown). Therefore, all vessels stained by the pan-endothelial marker CD31 were assumed to be blood vessels. In support of our hypothesis, the tumor area covered by CD31^{+} vessels was significantly reduced in ALCAM$^{-/-}$ mice, indicating a defect in tumor angiogenesis (Fig. 4H). Tumor blood vessels are known to grow in an uncontrolled manner and typically display a less mature phenotype, as manifested by reduced pericyte coverage [35]. When co-staining tumor nodule sections for the pericyte marker melanoma-associated antigen NG2 (NG2) [35, 36] and CD31, we observed that the vasculature of ALCAM$^{-/-}$ mice displayed an increased number of mature, i.e. NG2^{+} vessels (Fig. 4I). Overall, these findings suggested that, in comparison to the tumor vasculature of WT mice, ALCAM$^{-/-}$ mice displayed less aberrant tumor neoangiogenesis. Notably, numbers of tumor-infiltrating F4/80^{+} and of F4/80^{+}CD206^{+} M2-like macrophages [37], which are considered pro-angiogenic [38], were similar in both genotypes (Fig. S3), indicating that these cells did not contribute to the differences in tumor neovascularization observed between WT and ALCAM$^{-/-}$ mice.

316 **Stromal ALCAM deficiency reduces LLC homing and tumor growth in the lungs**

317 To confirm the observed tumor growth defect in a further model, we performed similar
318 intravenous metastasis studies using LLC cells, which express high levels of ALCAM (Fig. 5A).
319 Also upon LLC injection, a growth defect at the level of single tumor nodules was observed in the
320 lungs of ALCAM$^{-/-}$ compared to WT mice (Fig. 5B/C). Moreover, in comparison to WT mice, total
321 numbers of LLC tumor nodules were significantly reduced in the lungs of ALCAM$^{-/-}$ mice (Fig.
322 5D). To investigate potential differences in tumor cell seeding to the lung, we injected
323 fluorescently labeled LLC i.v. and quantified tumor cell numbers in the lungs after 24 hours by
324 FACS. This analysis revealed that LLC homing was significantly reduced into the lungs of
325 ALCAM$^{-/-}$ compared to WT mice (Fig. 5E,F).
326
327 **Stromal ALCAM deficiency leads to reduced spontaneous metastases to the lung and to**
328 **tumor-draining LNs**

329 In a next step we set out to investigate the metastatic process in a more physiological context. To
330 this end, luciferase-expressing LLC cells were subcutaneously (s.c.) implanted in the flank of WT
331 and ALCAM$^{-/-}$ mice and tumors were allowed to grow for 21-24 days. Subsequently, tumors were
332 resected, and spontaneous metastasis to different organs was analyzed three weeks later.
333 Surprisingly, s.c. implanted primary LLC tumors displayed a moderate growth advantage in
334 ALCAM$^{-/-}$ compared to WT control mice (Fig. 6A,B). No difference in blood vessel density was
335 observed in primary tumors of ALCAM$^{-/-}$ and WT mice (Fig. 6C). In fact, we could not detect
336 ALCAM in the LLC tumor vasculature (Fig. 6D), in line with our previous observation that ALCAM
337 is not expressed in the murine dermal vasculature under physiological conditions (Fig. 1D). To
338 allow for a better comparison of the spontaneous metastasis process, groups of mice with
339 similarly sized tumors were created. Specifically, only WT and ALCAM$^{-/-}$ mice with primary tumors
340 ranging from 200-1000 mg at the time point of resection were selected and kept in the study (Fig.
341 6E). Three weeks after primary tumor resection, all animals were sacrificed and luciferase activity
342 in the lung, liver and inguinal lymph nodes (LNs) was measured. This analysis revealed a

significant reduction in the overall metastatic burden in ALCAM$^{-/-}$ mice compared to WT controls (Fig. 6F-J and Fig. S4). In agreement with the reduced number of tumor nodules and tumor cell homing observed upon i.v. injection of LLC (Fig. 5D-F), a dramatic reduction in tumor metastasis to the lungs was observed in ALCAM$^{-/-}$ mice (Fig. 6H). Interestingly, metastasis to tumor-draining LNs was also significantly reduced (Fig. 6I), whereas no difference in the rate of metastasis to the liver was observed (Fig. 6J). Taken together, our work reveals a novel contribution of stromally expressed ALCAM in supporting metastatic spread and tumor outgrowth in the lungs and tumor-draining LNs.

Discussion

In this study we have investigated whether and how expression of ALCAM by cells that form the stromal tumor microenvironment contributes to tumor growth and metastatic spread. In the past, various studies have already documented the relevance of tumor cell-expressed ALCAM to tumor cell migration and invasion [25, 39-41], and metastasis [3, 23, 25]. On the other hand, several studies have reported on the expression and function of ALCAM in leukocytes [6-8, 10] and in endothelial cells [8, 11, 12, 26]. Since these cells are important constituents of the tumor stroma, the latter findings indirectly already suggested a more complex role of ALCAM in tumor growth and progression. Using ALCAM-deficient mice we now show for the first time that not only tumor cell-expressed but also stromally-expressed ALCAM may alter tumor growth and metastatic spread by affecting tumor angiogenesis and tumor cell homing.

Performing experiments in three different intravenous pulmonary metastasis models (i.e. B16F10, LLC and MC38) we observed that tumor growth in the lung was consistently reduced in ALCAM$^{-/-}$ compared to WT mice. Expansion of tumors is highly dependent on the formation of blood vessels [42]. Analyzing the blood vasculature in the lungs and in the diaphragm of ALCAM$^{-/-}$ mice we could show that loss of ALCAM indeed compromised the formation of the blood vascular network *in vivo*. This finding was further substantiated by our immunohistological analysis of lung tumor nodules in the MC38 metastasis model, which confirmed that the reduced tumor growth observed in ALCAM$^{-/-}$ mice was associated with a defect in tumor angiogenesis: Absence of ALCAM expression on stromal cells led to a reduction in tumor blood vessel density and increased the proportion of mature and likely quiescent vessels. Whether this angiogenesis defect is entirely dependent on the lack of ALCAM expression in the blood vasculature or potentially also supported by the lack of ALCAM on other stromal cells will need to be explored further.

Our findings revealed that the blood vasculature was compromised in the lung of ALCAM$^{-/-}$ mice. This might suggest that the reduced metastatic burden observed in our i.v. metastasis models could simply be explained by anatomic differences in the lungs of ALCAM$^{-/-}$ compared to WT

mice. However, we did not observe that tumor nodule numbers were consistently decreased in ALCAM$^{-/-}$ mice in the three different i.v. metastasis models investigated. In fact, a significant reduction in tumor nodule numbers and in tumor cell homing was only observed with LLC, both upon i.v. injection of tumor cells (Fig. 5E,F) as well as in the more physiological model of spontaneous metastasis from s.c. grafted primary tumors (Fig. 6H). This argues against a mere anatomic explanation for the reduced metastatic burden observed in the lungs of ALCAM$^{-/-}$ mice. The exact molecular interaction partners that could account for the homing defect observed in the case of LLC are not clear at this point. ALCAM is known to engage into homophilic as well as heterophilic interactions [4-6]. Given that LLC and B16F10 cells expressed similar levels of ALCAM (Fig. 5A & 3F), but a homing defect was only observed in the LLC model (Fig. 5E,F and Fig. S2), it is likely that tumor cell homing to the lungs does not depend on homophilic ALCAM-ALCAM interactions. Therefore, differential expression of other ALCAM binding partners [4-6] might explain the differences in the ALCAM dependence of tumor cell homing to the lung that was observed in the B16F10 and LLC models. Of interest in this regard is another study which has recently identified a role for the ALCAM binding partner L1CAM in the adhesion of breast cancer cells to ALCAM-expressing blood vascular endothelium *in vitro* [43]. However, we presently do not know whether differences in L1CAM expression might explain the homing phenotypes observed in our models. Moreover, besides L1CAM or other ALCAM binding partners, also other adhesion molecules expressed on the tumor cells could compensate for loss of endothelial ALCAM expression during tumor cell homing. Finally, it is also possible that alterations in tumor cell homing might be caused indirectly by leukocytes that contribute to the tumor cell extravasation process [33, 44-48].

Surprisingly we found that the growth of s.c. grafted primary tumors was slightly increased in ALCAM$^{-/-}$ compared to WT mice. In contrast to the angiogenesis defect observed in the lungs, which likely resulted in reduced growth of pulmonary tumor nodules, angiogenesis was not compromised in s.c. grafted tumors (Fig. 6C). This is in line with our observation that in mice ALCAM is not expressed in the vasculature of the dermis or of s.c. grafted tumors. The fact that

405 loss of ALCAM had an overall growth-promoting effect on s.c. grafted tumors suggests that
406 ALCAM expression in the tumor stroma not only supports angiogenesis (if expressed in the
407 vasculature), but also exerts tumor-suppressive functions. Although not further investigated in this
408 study, it is likely that loss of ALCAM might compromise the anti-tumor immune response. For
409 example, ALCAM was shown to support T cell activation, by stabilizing the immunologic synapse
410 [9, 10, 49]. Moreover, ALCAM has been implicated in leukocyte extravasation across blood vascular
411 endothelium [7, 8]. Interestingly, besides reducing spontaneous metastasis from primary LLC
412 tumors to the lungs (Fig. 6H), loss of ALCAM also appeared to reduce the rate of LLC metastasis
413 to draining LNs (Fig. 6I), but not to the liver (Fig. 6J). We have previously detected ALCAM
414 expression in the vasculature of the skin-draining LNs and in the liver ([11] and data not shown).
415 The reason why ALCAM deficiency did not affect LLC metastasis to the liver is unclear, but could
416 be linked with the expression of other adhesion molecules in the hepatic vasculature, which
417 might compensate for loss of ALCAM, or with the special blood flow conditions in the liver. In the
418 case of LN metastasis, it remains unclear at this point whether metastasis occurred via the blood
419 vasculature, or rather via tumor-draining lymphatic vessels. Given that the murine dermal
420 vasculature does not express ALCAM, a defect in lymphatic migration of tumor cells could only
421 have occurred at the level of the ALCAM-positive lymphatics in the LN. It is worth noticing that in
422 the lung and also in the diaphragm we found ALCAM to be higher expressed in lymphatic vessels
423 compared to blood vessels (Fig. 1C and data not shown). Thus, it is perceivable that in other
424 murine tissues, or in human skin in which ALCAM is expressed in the lymphatic vasculature ([11]
425 and Fig. 1A), ALCAM expression by (peri)tumoral lymphatics might directly impact tumor cell
426 metastasis to draining LNs.
427 Overall, our data reveal a novel contribution of stromal ALCAM expression to tumor growth and
428 metastatic spread and suggest an important role of ALCAM expressed in blood vessels in
429 supporting tumor angiogenesis. Moreover, our findings reveal that ALCAM expression in the lung
430 may additionally support tumor cell homing and seeding to this organ. These findings suggest
431 that ALCAM blockade could be beneficial for inhibiting tumor cell metastasis and tumor

(lymph)angiogenesis. The fact that we detected ALCAM expression in the vasculature of human lung and skin (Fig. 1A,B) strengthens the potential translational relevance of our findings.

Acknowledgement

We thank Simone Haener (ETH Zurich) for excellent technical assistance and the staff of the ETH Zurich Rodent Center HCI (RCHCI) and University of Zurich Laboratory Animal Service Center (LASC) for animal husbandry. CH gratefully acknowledges financial support from the Swiss National Science Foundation (grants 310030_138330 and 310030_156269) and the Promedica Foundation (Chur, Switzerland).

References

[1] Cavallaro U, Christofori G: Cell adhesion and signalling by cadherins and Ig-CAMs in cancer. Nat Rev Cancer 2004, 4:118-32.

[2] Reymond N, d'Agua BB, Ridley AJ: Crossing the endothelial barrier during metastasis. Nat Rev Cancer 2013, 13:858-70.

[3] Wai Wong C, Dye DE, Coombe DR: The role of immunoglobulin superfamily cell adhesion molecules in cancer metastasis. Int J Cell Biol 2012, 2012:340296.

[4] Buhusi M, Demyanenko GP, Jannie KM, Dalal J, Darnell EP, Weiner JA, Maness PF: ALCAM regulates mediolateral retinotopic mapping in the superior colliculus. J Neurosci 2009, 29:15630-41.

[5] Delgado VM, Nugnes LG, Colombo LL, Troncoso MF, Fernandez MM, Malchiodi EL, Frahm I, Croci DO, Compagno D, Rabinovich GA, Wolfenstein-Todel C, Elola MT: Modulation of endothelial cell migration and angiogenesis: a novel function for the "tandem-repeat" lectin galectin-8. FASEB J 2011, 25:242-54.

[6] Aruffo A, Bowen MA, Patel DD, Haynes BF, Starling GC, Gebe JA, Bajorath J: CD6-ligand interactions: a paradigm for SRCR domain function? Immunol Today 1997, 18:498-504.

[7] Cayrol R, Wosik K, Berard JL, Dodelet-Devillers A, Ifergan I, Kebir H, Haqqani AS, Kreymborg K, Krug S, Moumdjian R, Bouthillier A, Becher B, Arbour N, David S, Stanimirovic D, Prat A: Activated leukocyte cell adhesion molecule promotes leukocyte trafficking into the central nervous system. Nat Immunol 2008, 9:137-45.

[8] Masedunskas A, King JA, Tan F, Cochran R, Stevens T, Sviridov D, Ofori-Acquah SF: Activated leukocyte cell adhesion molecule is a component of the endothelial junction involved in transendothelial monocyte migration. FEBS Lett 2006, 580:2637-45.

[9] Hassan NJ, Barclay AN, Brown MH: Frontline: Optimal T cell activation requires the engagement of CD6 and CD166. Eur J Immunol 2004, 34:930-40.

[10] Zimmerman AW, Joosten B, Torensma R, Parnes JR, van Leeuwen FN, Figdor CG: Long-term engagement of CD6 and ALCAM is essential for T-cell proliferation induced by dendritic cells. Blood 2006, 107:3212-20.

471 [11] Iolyeva M, Karaman S, Willrodt AH, Weingartner S, Vigl B, Halin C: Novel role for ALCAM in
472 lymphatic network formation and function. FASEB J 2013, 27:978-90.
473 [12] Ikeda K, Quertermous T: Molecular isolation and characterization of a soluble isoform of
474 activated leukocyte cell adhesion molecule that modulates endothelial cell function. J Biol
475 Chem 2004, 279:55315-23.
476 [13] Lecuyer MA, Saint-Laurent O, Bourbonniere L, Larouche S, Larochelle C, Michel L,
477 Charabati M, Abadier M, Zandee S, Haghayegh Jahromi N, Gowing E, Pittet C, Lyck R,
478 Engelhardt B, Prat A: Dual role of ALCAM in neuroinflammation and blood-brain barrier
479 homeostasis. Proc Natl Acad Sci U S A 2017, 114:E524-E33.
480 [14] Ofori-Acquah SF, King J, Voelkel N, Schaphorst KL, Stevens T: Heterogeneity of barrier
481 function in the lung reflects diversity in endothelial cell junctions. Microvasc Res 2008,
482 75:391-402.
483 [15] Schliemann C, Roesli C, Kamada H, Borgia B, Fugmann T, Klapper W, Neri D: In vivo
484 biotinylation of the vasculature in B-cell lymphoma identifies BST-2 as a target for antibody-
485 based therapy. Blood 2010, 115:736-44.
486 [16] Weiner JA, Koo SJ, Nicolas S, Fraboulet S, Pfaff SL, Pourquie O, Sanes JR: Axon
487 fasciculation defects and retinal dysplasias in mice lacking the immunoglobulin superfamily
488 adhesion molecule BEN/ALCAM/SC1. Mol Cell Neurosci 2004, 27:59-69.
489 [17] Patel DD, Wee SF, Whichard LP, Bowen MA, Pesando JM, Aruffo A, Haynes BF:
490 Identification and characterization of a 100-kD ligand for CD6 on human thymic epithelial
491 cells. J Exp Med 1995, 181:1563-8.
492 [18] Singer NG, Mitra R, Lialios F, Richardson BC, Marks RM, Pesando JM, Fox DA, Nickoloff
493 BJ: CD6 dependent interactions of T cells and keratinocytes: functional evidence for a
494 second CD6 ligand on gamma-interferon activated keratinocytes. Immunol Lett 1997, 58:9-
495 14.
496 [19] Ye M, Du YL, Nie YQ, Zhou ZW, Cao J, Li YF: Overexpression of activated leukocute cell
497 adhesion molecule in gastric cancer is associated with advanced stages and poor prognosis
498 and miR-9 deregulation. Mol Med Rep 2015, 11:2004-12.

[20] Weichert W, Knosel T, Bellach J, Dietel M, Kristiansen G: ALCAM/CD166 is overexpressed in colorectal carcinoma and correlates with shortened patient survival. J Clin Pathol 2004, 57:1160-4.

[21] Hansen AG, Freeman TJ, Arnold SA, Starchenko A, Jones-Paris CR, Gilger MA, Washington MK, Fan KH, Shyr Y, Beauchamp RD, Zijlstra A: Elevated ALCAM shedding in colorectal cancer correlates with poor patient outcome. Cancer Res 2013, 73:2955-64.

[22] Kahlert C, Weber H, Mogler C, Bergmann F, Schirmacher P, Kenngott HG, Matterne U, Mollberg N, Rahbari NN, Hinz U, Koch M, Aigner M, Weitz J: Increased expression of ALCAM/CD166 in pancreatic cancer is an independent prognostic marker for poor survival and early tumour relapse. Br J Cancer 2009, 101:457-64.

[23] Hansen AG, Arnold SA, Jiang M, Palmer TD, Ketova T, Merkel A, Pickup M, Samaras S, Shyr Y, Moses HL, Hayward SW, Sterling JA, Zijlstra A: ALCAM/CD166 is a TGF-beta-responsive marker and functional regulator of prostate cancer metastasis to bone. Cancer Res 2014, 74:1404-15.

[24] Kristiansen G, Pilarsky C, Wissmann C, Kaiser S, Bruemmendorf T, Roepcke S, Dahl E, Hinzmann B, Specht T, Pervan J, Stephan C, Loening S, Dietel M, Rosenthal A: Expression profiling of microdissected matched prostate cancer samples reveals CD166/MEMD and CD24 as new prognostic markers for patient survival. J Pathol 2005, 205:359-76.

[25] van Kempen LC, van den Oord JJ, van Muijen GN, Weidle UH, Bloemers HP, Swart GW: Activated leukocyte cell adhesion molecule/CD166, a marker of tumor progression in primary malignant melanoma of the skin. Am J Pathol 2000, 156:769-74.

[26] Degen WG, van Kempen LC, Gijzen EG, van Groningen JJ, van Kooyk Y, Bloemers HP, Swart GW: MEMD, a new cell adhesion molecule in metastasizing human melanoma cell lines, is identical to ALCAM (activated leukocyte cell adhesion molecule). Am J Pathol 1998, 152:805-13.

[27] Donizy P, Zietek M, Halon A, Leskiewicz M, Kozyra C, Matkowski R: Prognostic significance of ALCAM (CD166/MEMD) expression in cutaneous melanoma patients. Diagn Pathol 2015, 10:86.

527 [28] Balkwill FR, Capasso M, Hagemann T: The tumor microenvironment at a glance. J Cell Sci
528 2012, 125:5591-6.
529 [29] Whiteside TL: The tumor microenvironment and its role in promoting tumor growth.
530 Oncogene 2008, 27:5904-12.
531 [30] Zhang J, Liu J: Tumor stroma as targets for cancer therapy. Pharmacol Ther 2013, 137:200-
532 15.
533 [31] Corbett TH, Griswold DP, Jr., Roberts BJ, Peckham JC, Schabel FM, Jr.: Tumor induction
534 relationships in development of transplantable cancers of the colon in mice for chemotherapy
535 assays, with a note on carcinogen structure. Cancer Res 1975, 35:2434-9.
536 [32] Hoos A, Protsyuk D, Borsig L: Metastatic growth progression caused by PSGL-1-mediated
537 recruitment of monocytes to metastatic sites. Cancer Res 2014, 74:695-704.
538 [33] Wolf MJ, Hoos A, Bauer J, Boettcher S, Knust M, Weber A, Simonavicius N, Schneider C,
539 Lang M, Sturzl M, Croner RS, Konrad A, Manz MG, Moch H, Aguzzi A, van Loo G,
540 Pasparakis M, Prinz M, Borsig L, Heikenwalder M: Endothelial CCR2 signaling induced by
541 colon carcinoma cells enables extravasation via the JAK2-Stat5 and p38MAPK pathway.
542 Cancer Cell 2012, 22:91-105.
543 [34] Arbiser JL, Moses MA, Fernandez CA, Ghiso N, Cao Y, Klauber N, Frank D, Brownlee M,
544 Flynn E, Parangi S, Byers HR, Folkman J: Oncogenic H-ras stimulates tumor angiogenesis
545 by two distinct pathways. Proc Natl Acad Sci U S A 1997, 94:861-6.
546 [35] Morikawa S, Baluk P, Kaidoh T, Haskell A, Jain RK, McDonald DM: Abnormalities in
547 pericytes on blood vessels and endothelial sprouts in tumors. Am J Pathol 2002, 160:985-
548 1000.
549 [36] Ozerdem U, Grako KA, Dahlin-Huppe K, Monosov E, Stallcup WB: NG2 proteoglycan is
550 expressed exclusively by mural cells during vascular morphogenesis. Dev Dynam 2001,
551 222:218-27.
552 [37] Stein M, Keshav S, Harris N, Gordon S: Interleukin 4 potently enhances murine macrophage
553 mannose receptor activity: a marker of alternative immunologic macrophage activation. J Exp
554 Med 1992, 176:287-92.

555 [38] Chambers SE, O'Neill CL, O'Doherty TM, Medina RJ, Stitt AW: The role of immune-related
556 myeloid cells in angiogenesis. Immunobiology 2013, 218:1370-5.
557 [39] Jannie KM, Stipp CS, Weiner JA: ALCAM regulates motility, invasiveness, and adherens
558 junction formation in uveal melanoma cells. PLoS One 2012, 7:e39330.
559 [40] Ishiguro F, Murakami H, Mizuno T, Fujii M, Kondo Y, Usami N, Yokoi K, Osada H, Sekido Y:
560 Activated leukocyte cell-adhesion molecule (ALCAM) promotes malignant phenotypes of
561 malignant mesothelioma. J Thorac Oncol 2012, 7:890-9.
562 [41] Lunter PC, van Kilsdonk JW, van Beek H, Cornelissen IM, Bergers M, Willems PH, van
563 Muijen GN, Swart GW: Activated leukocyte cell adhesion molecule (ALCAM/CD166/MEMD),
564 a novel actor in invasive growth, controls matrix metalloproteinase activity. Cancer Res 2005,
565 65:8801-8.
566 [42] Hanahan D, Weinberg RA: Hallmarks of cancer: the next generation. Cell 2011, 144:646-74.
567 [43] Dippel V, Milde-Langosch K, Wicklein D, Schumacher U, Altevogt P, Oliveira-Ferrer L,
568 Janicke F, Schroder C: Influence of L1-CAM expression of breast cancer cells on adhesion
569 to endothelial cells. J Cancer Res Clin Oncol 2013, 139:107-21.
570 [44] Zhao L, Lim SY, Gordon-Weeks AN, Tapmeier TT, Im JH, Cao Y, Beech J, Allen D, Smart S,
571 Muschel RJ: Recruitment of a myeloid cell subset (CD11b/Gr1 mid) via CCL2/CCR2
572 promotes the development of colorectal cancer liver metastasis. Hepatology 2013, 57:829-
573 39.
574 [45] Cassetta L, Pollard JW: Cancer immunosurveillance: role of patrolling monocytes. Cell Res
575 2016, 26:3-4.
576 [46] Qian B, Deng Y, Im JH, Muschel RJ, Zou Y, Li J, Lang RA, Pollard JW: A distinct
577 macrophage population mediates metastatic breast cancer cell extravasation, establishment
578 and growth. PLoS One 2009, 4:e6562.
579 [47] Morvan MG, Lanier LL: NK cells and cancer: you can teach innate cells new tricks. Nat Rev
580 Cancer 2016, 16:7-19.
581 [48] Coffelt SB, Wellenstein MD, de Visser KE: Neutrophils in cancer: neutral no more. Nat Rev
582 Cancer 2016, 16:431-46.

583 [49] Hassan NJ, Simmonds SJ, Clarkson NG, Hanrahan S, Puklavec MJ, Bomb M, Barclay AN,
584 Brown MH: CD6 regulates T-cell responses through activation-dependent recruitment of the
585 positive regulator SLP-76. Mol Cell Biol 2006, 26:6727-38.
586

587 **Figure Legends**

588

589 **Figure 1: ALCAM is expressed in the human and murine vasculature and contributes to *in***
590 ***vitro* angiogenesis.** (**A,B**) Immunofluorescence analysis of human skin (A) and lung (B) tissue
591 sections, demonstrating expression of ALCAM in $CD31^+$ vessels. Row labeling: ALCAM staining;
592 performed with primary goat anti-ALCAM. Isotype staining: performed with primary goat isotype
593 control antibody. Scale bars: 100 µm. Representative images from n=3 (skin) and n=2 (lung)
594 different biopsy samples are shown (**C,D**) Single cell suspensions were generated from murine
595 lungs (C) and ear skin (D) and stained for CD31, podoplanin and CD45. Blood vascular
596 endothelial cells (BECs) and lymphatic endothelial cells (LECs) were identified by gating on
597 $CD45^-CD31^+podoplanin^-$ (BECs) or $CD45^-CD31^+podoplanin^+$ (LECs) cells, respectively. Black
598 open histogram: αALCAM staining; grey tinted histogram: isotype control. Representative data
599 from one out of three similar experiments are shown. (**E,F**) FACS analysis of ALCAM expression
600 in (**E**) HUVECs and (**F**) MS-1 cells. Black open histogram: αALCAM staining; grey tinted
601 histogram: isotype control. (**G,H**) Scratch-wound assay: A cell-free zone was introduced into
602 confluent HUVEC or MS-1 monolayers and the effect of ALCAM blockade on scratch closure,
603 which represents migration of bordering LECs into the cell-free zone, was analyzed 12 hours
604 later. (**G**) Representative images taken from an experiment with performed HUVECS (**H**) Results
605 from HUVEC and MS-1 scratch assays. Data from one out of three (HUVEC) or five (MS-1)
606 experiments are shown. $^{**}P < 0.01$, $^{***}P < 0.001$

607

608 **Figure 2: $ALCAM^{-/-}$ mice display an abnormal vascular phenotype in the diaphragm and the**
609 **lung *in vivo*.** (**A-B**) PFA-fixed diaphragms of six-day-old WT or $ALCAM^{-/-}$ pups were
610 immunofluorescently stained for the panendothelial marker CD31. To analyze blood vessels only,
611 $CD31^+$ lymphatic vessels (identified by their $CD31^{dim}$ staining and large vessel diameter) were
612 removed from the image using ImageJ software. (**A**) Representative images taken from WT and
613 $ALCAM^{-/-}$ diaphragms. Scale bar = 200 µm. Quantification of (**B**) the total area covered by $CD31^+$

614 blood vessels and (**C**) the diameter of $CD31^+$ blood vessels. N=7-9 mice per group. (**D-L**)**:**
615 Image-based morphometric analysis to quantify (**D**) vWF stainings in PFA-fixed lung sections of
616 WT or $ALCAM^{-/-}$ mice. vWF: scale bar = 200 μm and (**E**) Analysis of the average size if vWF^+
617 vessels. (**F**) αSMA stainings in PFA-fixed lung sections of WT or $ALCAM^{-/-}$ mice. ; αSMA: scale
618 bar = 200 μm. (**G**) Analysis of the average size of αSMA^+ vessels. (**H**) Analysis of the number of
619 αSMA^+ vessels in WT and $ALCAM^{-/-}$ mice. vWF: n=3 mice per group, αSMA: n=4-5 mice per
620 group. **P* < 0.05, ***P* < 0.01, ****P* < 0.001
621
622 **Figure 3: Stromal ALCAM deficiency reduces lung metastasis growth in B16F10 model.**
623 Mice were injected i.v. with luciferase-expressing $1x10^6$ B16F10 tumor cells and (**A**) tumor growth
624 was monitored over time by IVIS-based analysis of *in vivo* luciferase activity. (**B**) Representative
625 images of lungs from WT and $ALCAM^{-/-}$ mice at the end of the study, revealing the coverage with
626 melanin-producing B16F10 tumor cells. (**C,D**) IVIS-based analysis of *ex vivo* luciferase activity in
627 (**C**) excised lungs and (**D**) lung homogenates. (**E**) Manual counting of visible lung metastases. (**F**)
628 FACS analysis of ALCAM expression of *in vitro*-cultured B16F10. Black histogram: anti-ALCAM
629 staining; grey histogram: isotype control. (**G**) Assessment of the area covered by visible
630 metastases (mets). (**H**) Distribution of small (white; diameter < 200 μm), medium (grey; diameter
631 < 350 μm) and large (black; diameter > 350 μm) metastases in lungs of WT or $ALCAM^{-/-}$ mice. (A-
632 H) N=9-10 mice per group. Data from one out of three similar experiments are shown. ***P* < 0.01,
633 ****P* < 0.001
634
635 **Figure 4: Stromal ALCAM deficiency reduces MC38 tumor growth and angiogenesis.** Mice
636 were i.v. injected with $3x10^5$ MC38 tumor cells and the tumor burden was quantified after 24-26
637 days. (**A**) FACS analysis of ALCAM expression by *in vitro*-cultured MC38 cells. Black histogram:
638 anti-ALCAM staining; grey histogram: isotype control. (**B**) Representative images of tumor-
639 bearing lungs of WT and $ALCAM^{-/-}$ mice. (**C**) Quantification of the number of metastases (mets).
640 (**D**) Average weight of the twelve biggest excised metastases per mouse. Pooled data from three

similar experiments involving a total of 17-18 mice per group are shown. Data are represented as mean ± SEM. (**E-G**) Sections of the 12 biggest metastases were stained with H&E and (**E**) average metastasis size was measured. (**F,G**) Metastases were grouped into the categories "small" (white; diameter < 2.5 mm) or "large" (black, diameter > 2.5 mm). (**F**) Representative images of a small and a large metastasis**.** Scale bar = 1 mm. (**G**) Percentage-based distribution of metastasis sizes according to the genotype. (**H**) Metastases sections were stained for CD31 and the $CD31^+$ area was quantified. Scale bar = 200 μm. (**I**) Metastases sections were stained for CD31 and NG2. The percentage of $CD31^+NG2^+$ amongst all $CD31^+$ vessels was quantified. (E-I) N=4-5 mice per group. Data from one experiment are shown. $^*P < 0.05$, $^{**}P < 0.01$, $^{***}P < 0.001$

Figure 5: Stromal ALCAM deficiency reduces LLC homing and tumor growth in the lungs. (**A**) FACS analysis of ALCAM expression of *in vitro*-cultured LLC. Black open histogram: αALCAM staining; grey tinted histogram: isotype control. (**B,C**): WT and $ALCAM^{-/-}$ mice were injected i.v. with LLC ($1.5x10^5$) cells, and the metastatic burden in the lung was analyzed on day 12-14. (**B**) Images of tumor-bearing lungs at the end of the study. (**C**) Average weight of all excised metastases. (**D**) Total number of metastases in WT compared to $ALCAM^{-/-}$ mice. (B-C) N=16 mice per group. Pooled data from two independent experiments are shown. (**E,F**) Mice were injected with CFSE-labeled LLC cells ($1x10^6$) i.v. followed by FACS analysis of lung single-cell suspensions after 24 hours. (**E**) Gating scheme: Tumor cells were identified by gating on $CD45^-$ $CFSE^+$ cells. (**F**) Quantification of $CD45^-$ $CFSE^+$ LLC tumor cells. (E,F). Pooled data from three independent experiments are shown (N=24-25 mice per group). $^*P < 0.05$, $^{**}P < 0.01$, $^{***}P < 0.001$

Figure 6: Stromal ALCAM deficiency leads to reduced spontaneous metastases to the lung. (**A-D**) Mice were s.c. injected with $2x10^5$ luciferase-expressing LLC cells and primary tumors were resected after 21 to 24 days. (**A**) Primary tumor growth in WT and $ALCAM^{-/-}$ mice. (**B**) Quantification of the excised primary tumor weight. Each dot represents one mouse. (**A,B**)

Pooled data from two independent experiments are shown. N=28-29 mice per group. (**C**) Tumor vascularization was assessed by quantifying the area of $CD31^+$ vessels. Scale bar = 200 µm, n=16-19 mice per group. Pooled data from two independent experiments are. (**D**) FACS analysis of ALCAM expression on single cell suspensions of ECs ($CD45^-$ $CD31^+$) derived from lungs or from s.c. growing primary LLC tumors. Data from one out of three similar experiments shown. Black open histogram: αALCAM staining; grey tinted histogram: isotype control. (**E-I**) Mice with tumors ranging between 200-1000 mg on the day of resection were included in the subsequent study to monitor spontaneous metastasis. Mice were sacrificed 3 weeks after primary tumor resection and the metastatic burden was analyzed by IVIS-based measurement of luciferase activity in the respective organs, namely in lung, liver and inguinal LN. (**E**) Weights of the excised tumors from mice that were included in the spontaneous metastasis study. Each dot represents one mouse. (**F**) Quantification of the overall rate of metastasis in $ALCAM^{-/-}$ and in WT mice. Black: mice with metastases detected in at least one organ. White: mice with no detectable metastases. (**G**) Same as in (F), but revealing the distribution of metastases in specific organs. (**H-J**) Rates of (**H**) lung, (**I**) LN and (**J**) liver metastases in WT and $ALCAM^{-/-}$ mice. (E-I) Pooled data from two independent experiments are shown in. N=16-18 mice per group. $^*P < 0.05$, $^{***}P < 0.001$

Supplemental Figure 1: Analysis of ALCAM expression in endothelial cells and other stromal cells (**A, B**) High magnification confocal analysis of human lung tissue sections, demonstrating expression of ALCAM in $CD31^+$ endothelial cells but not in αSMA^+ mural cells. (**A**) CD31 - ALCAM colocalization. (**B**) αSMA (red) - ALCAM (white) colocalization. Row labeling: ALCAM staining; performed with primary goat anti-ALCAM. Isotype staining: performed with primary goat isotype control antibody. For all conditions, an overview image (left), a high magnification zoomed image (middle) and a corresponding orthogonal view (right) are shown. Scale bars: 100 µm (overview images) and 20 µm (zoomed images). Representative images from n=2 different lung biopsy samples are shown. (**C,D**) Single cell suspensions were generated from murine lungs and ALCAM expression was analyzed in endothelial cells ($CD45^-CD31^+$) and

695 other stromal cells ($CD45^-CD31^-$). (**C**) Depiction of the gating scheme. (**D**) Analysis or ALCAM
696 expression in four different stromal cell types (differentiated based on their expression of CD31
697 and podoplanin) was performed in WT and in $ALCAM^{-/-}$ mice (to confirm the specificity of the
698 staining). Black open histogram: anti-ALCAM staining; grey tinted histogram: isotype control.
699 Representative data from one out of two similar experiments are shown.
700
701 **Supplemental Figure 2: B16F10 cell homing to lungs of WT and $ALCAM^{-/-}$ mice.** Mice were
702 injected with CFSE-labeled B16F10 cells ($1x10^6$) i.v. 24 hours later, lungs were perfused and
703 FACS analysis was performed on lung single-cell suspensions. (**A**) FACS gating scheme: Tumor
704 cells were identified by gating on $CD45^-$ $CFSE^+$ cells. (**B**) Quantification of $CD45^-$ $CFSE^+$ LLC
705 tumor cells. Pooled data from three independent experiments are shown. N=9 mice per group.
706
707 **Supplemental Figure 3: $ALCAM^{-/-}$ mice do not display reduced macrophage infiltration into**
708 **the tumor.** Mice were s.c. injected with $2x10^5$ luciferase-expressing LLC cells and primary tumors
709 were resected after 21 to 24 days. (**A**) Metastases sections were stained for F4/80 and CD206.
710 Scale bar = 200 µm. Macrophage infiltration was analyzed by quantifying the tumor area covered
711 by (**B**) $F4/80^+$ cells and (**C**) $F4/80^+$ of $F4/80^+CD206^+$ double-positive (M2-like) macrophages.
712 Scale bar = 100 µm. N=4-5 mice per group. Data from one experiment are shown.
713
714 **Supplemental Figure 4: Reduced metastatic burden in $ALCAM^{-/-}$ mice.** Mice were s.c.
715 injected with $2x10^5$ LLC. Primary tumors were resected after 21 to 24 days. Three weeks after
716 primary tumor removal, metastases were identified by IVIS-based measurement of luciferase
717 activity in the respective organs: lung (upper left), liver (upper right) and inguinal LNs (bottom).
718 Pictures show pooled results from two independent studies. N=16-18 mice per group.
719

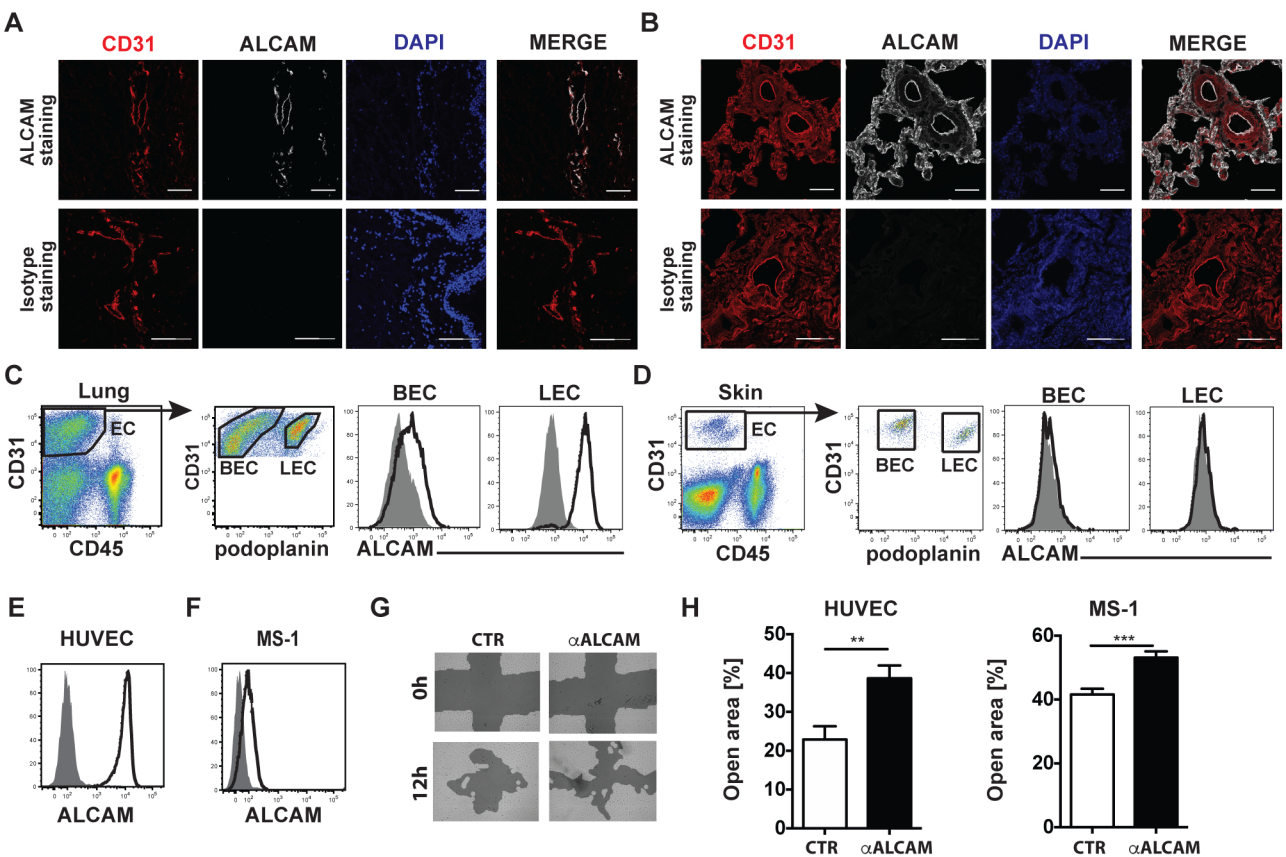
A
CD31
ALCAM
DAPI
MERGE
ALCAM staining
Isotype staining
B
CD31
ALCAM
DAPI
MERGE
ALCAM staining
Isotype staining
C
Lung
EC
CD31
CD45
BEC
LEC
CD31
podoplanin
BEC
LEC
ALCAM
D
Skin
EC
CD31
CD45
BEC
LEC
CD31
podoplanin
BEC
LEC
ALCAM
E
HUVEC
ALCAM
F
MS-1
ALCAM
G
CTR
αALCAM
0h
12h
H
HUVEC
Open area [%]
50
40
30
20
10
0
**
CTR
αALCAM
MS-1
Open area [%]
60
40
20
0
***
CTR
αALCAM

Figure 1

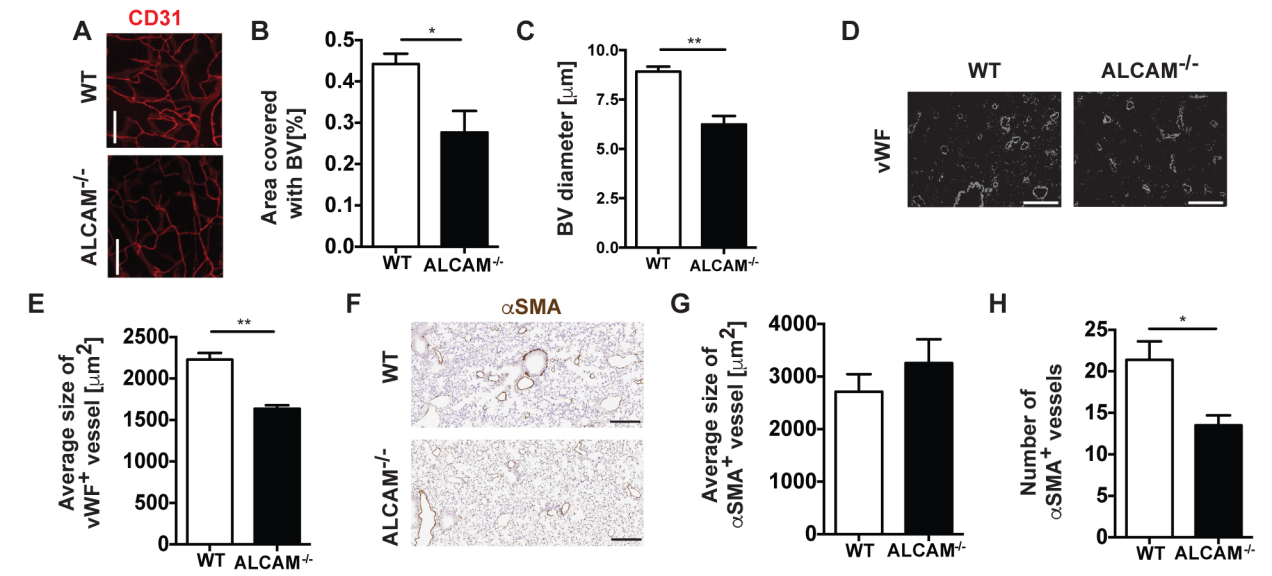
A
CD31
WT
ALCAM-/-
B
Area covered with BV[%]
0.5
0.4
0.3
0.2
0.1
0.0
*
WT
ALCAM-/-
C
BV diameter [μm]
10.0
7.5
5.0
2.5
0.0
**
WT
ALCAM-/-
D
WT
ALCAM-/-
vWF
E
Average size of vWF+ vessel [μm2]
2500
2000
1500
1000
500
0
**
WT
ALCAM-/-
F
αSMA
WT
ALCAM-/-
G
Average size of αSMA+ vessel [μm2]
4000
3000
2000
1000
0
WT
ALCAM-/-
H
Number of αSMA+ vessels
25
20
15
10
5
0
*
WT
ALCAM-/-

Figure 2

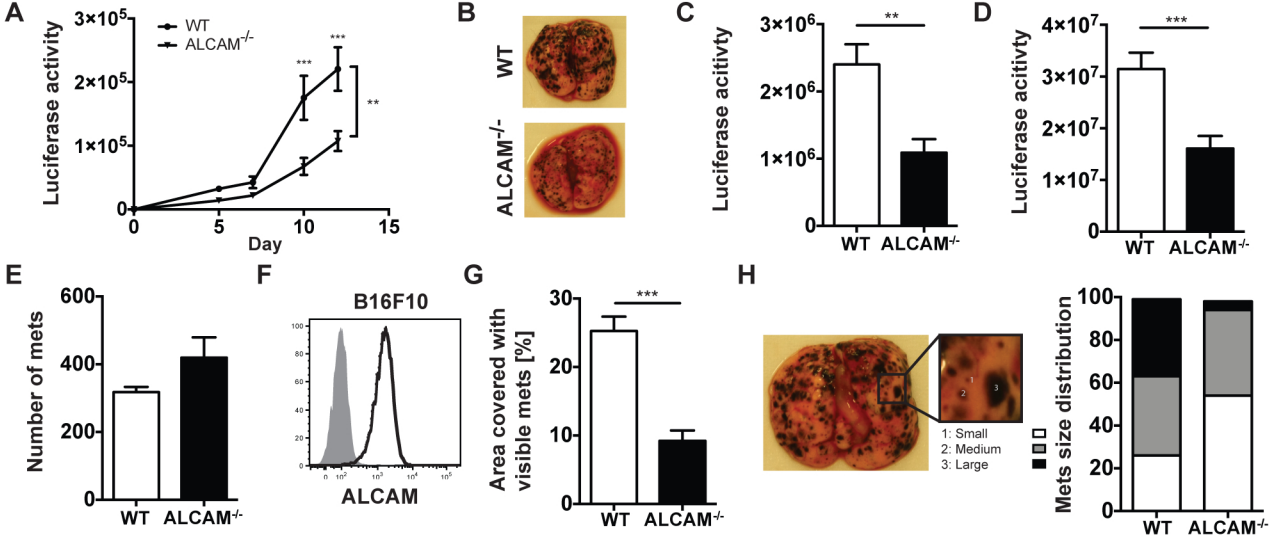
A
Luciferase activity
3×10^5
2×10^5
1×10^5
0
WT
ALCAM-/-
***
***
**
0
5
10
15
Day
B
WT
ALCAM-/-
C
Luciferase acitivty
3×10^6
2×10^6
1×10^6
0
**
WT
ALCAM-/-
D
Luciferase acitivty
4×10^7
3×10^7
2×10^7
1×10^7
0
***
WT
ALCAM-/-
E
Number of mets
600
400
200
0
WT
ALCAM-/-
F
B16F10
ALCAM
G
Area covered with visible mets [%]
30
20
10
0
***
WT
ALCAM-/-
H
1: Small
2: Medium
3: Large
Mets size distribution
100
80
60
40
20
0
WT
ALCAM-/-

Figure 3

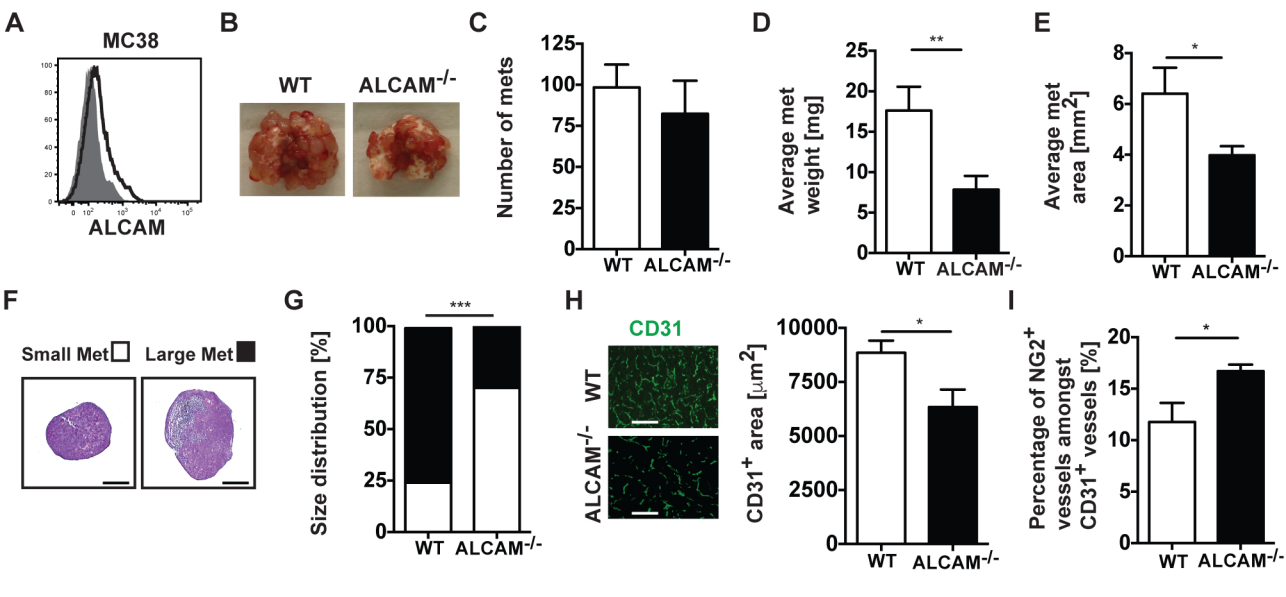
A
MC38
ALCAM
B
WT
ALCAM-/-
C
Number of mets
125
100
75
50
25
0
WT
ALCAM-/-
D
Average met weight [mg]
**
25
20
15
10
5
0
WT
ALCAM-/-
E
Average met area [mm2]
*
8
6
4
2
0
WT
ALCAM-/-
F
Small Met
Large Met
G
Size distribution [%]
***
100
75
50
25
0
WT
ALCAM-/-
H
CD31
WT
ALCAM-/-
CD31+ area [μm2]
*
10000
7500
5000
2500
0
WT
ALCAM-/-
I
Percentage of NG2+ vessels amongst CD31+ vessels [%]
*
20
15
10
5
0
WT
ALCAM-/-

Figure 4

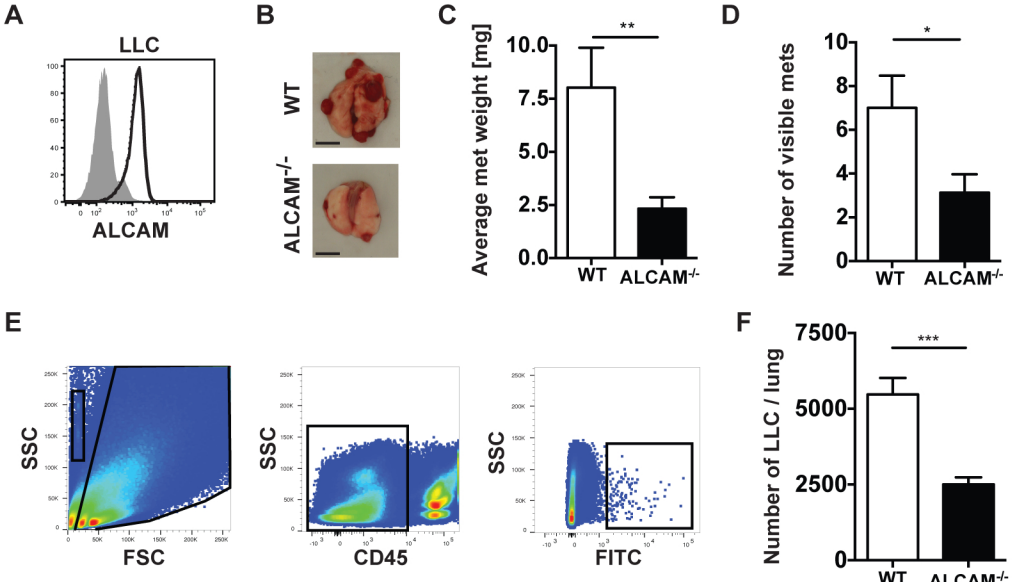
A
LLC
ALCAM
B
WT
ALCAM-/-
C
Average met weight [mg]
10.0
7.5
5.0
2.5
0.0
**
WT
ALCAM-/-
D
Number of visible mets
10
8
6
4
2
0
*
WT
ALCAM-/-
E
SSC
FSC
SSC
CD45
SSC
FITC
F
Number of LLC / lung
7500
5000
2500
0
***
WT
ALCAM-/-

Figure 5

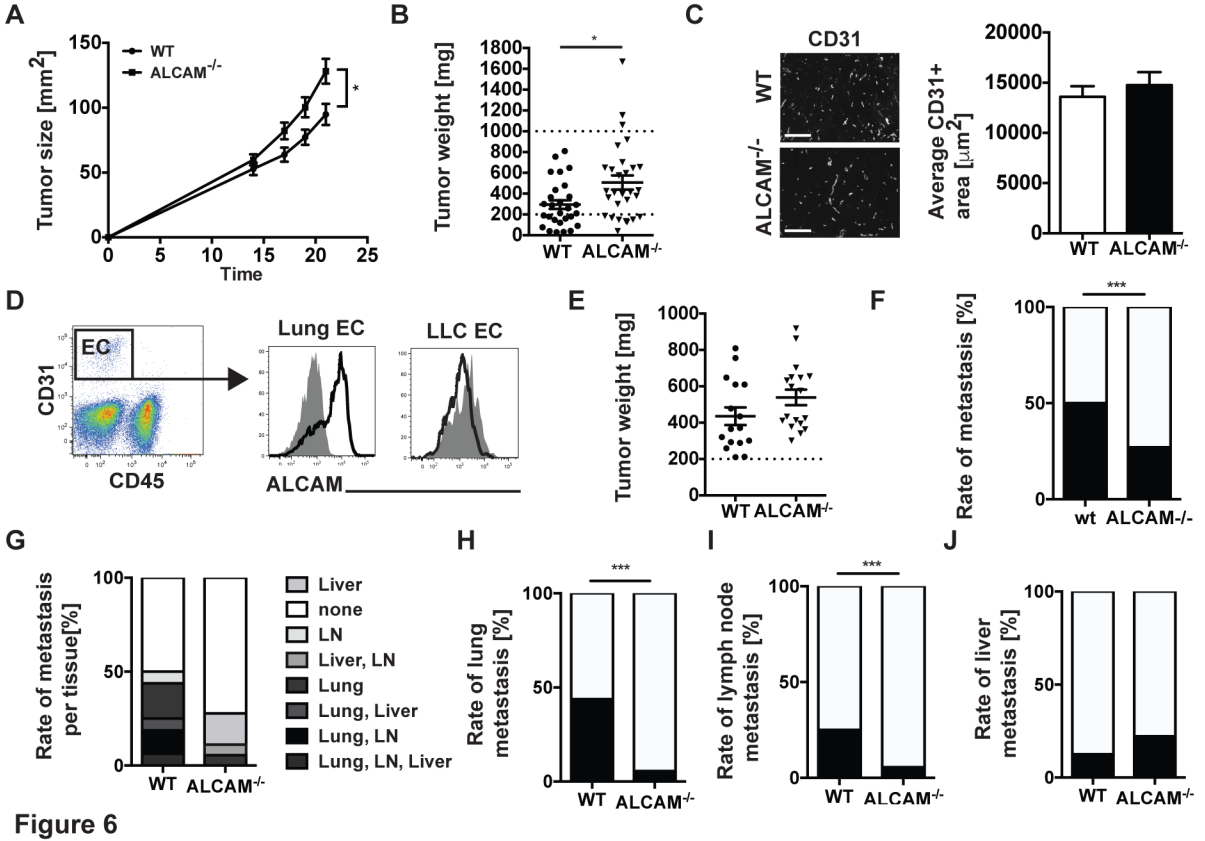
A
Tumor size [mm2]
WT
ALCAM-/-
Time
B
Tumor weight [mg]
WT ALCAM-/-
C
CD31
WT
ALCAM-/-
Average CD31+ area [μm2]
WT ALCAM-/-
D
EC
CD31
CD45
Lung EC
LLC EC
ALCAM
E
Tumor weight [mg]
WT ALCAM-/-
F
Rate of metastasis [%]
wt ALCAM-/-
G
Rate of metastasis per tissue[%]
WT ALCAM-/-
Liver
none
LN
Liver, LN
Lung
Lung, Liver
Lung, LN
Lung, LN, Liver
H
Rate of lung metastasis [%]
WT ALCAM-/-
I
Rate of lymph node metastasis [%]
WT ALCAM-/-
J
Rate of liver metastasis [%]
WT ALCAM-/-

Figure 6

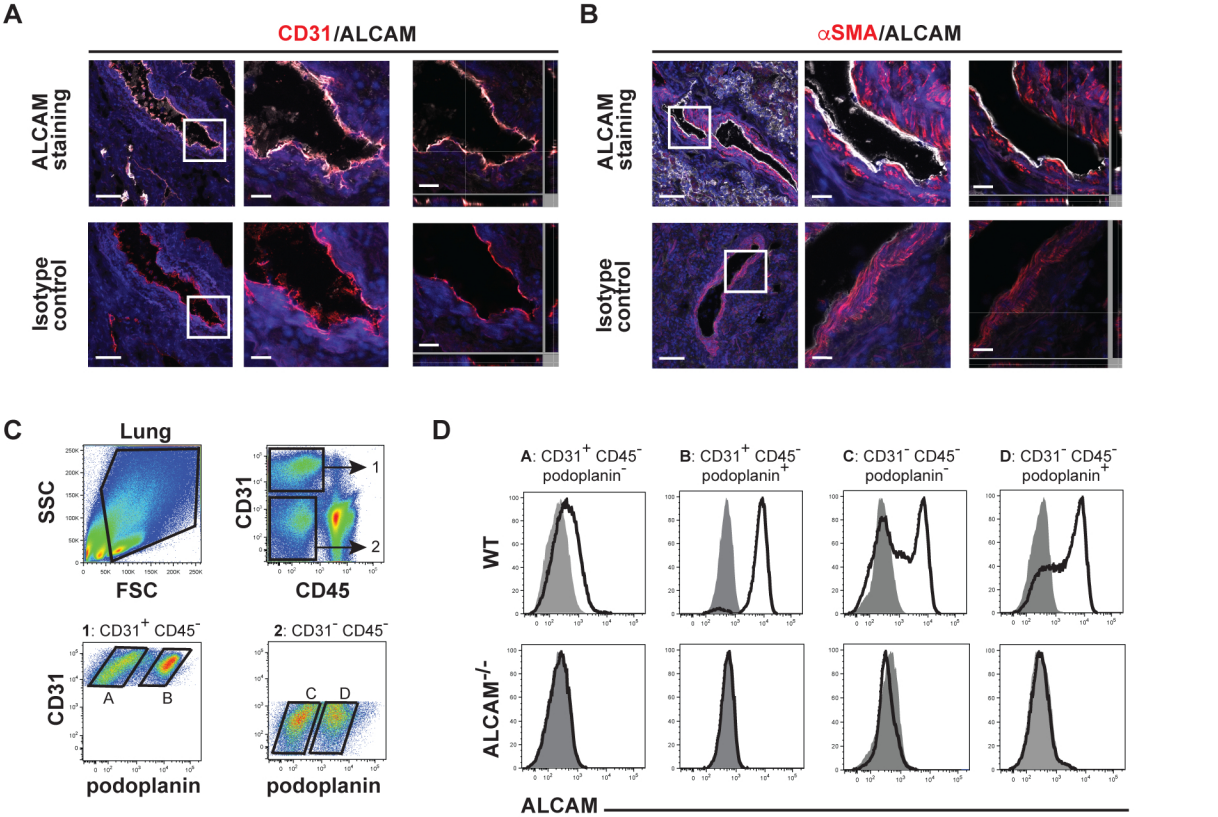

Supplemental Figure 1

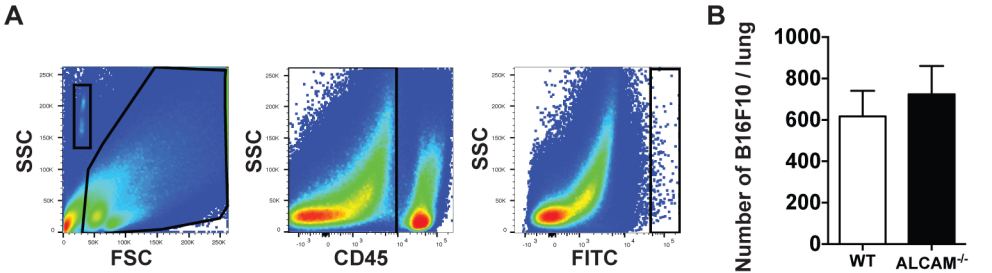

Supplemental Figure 2

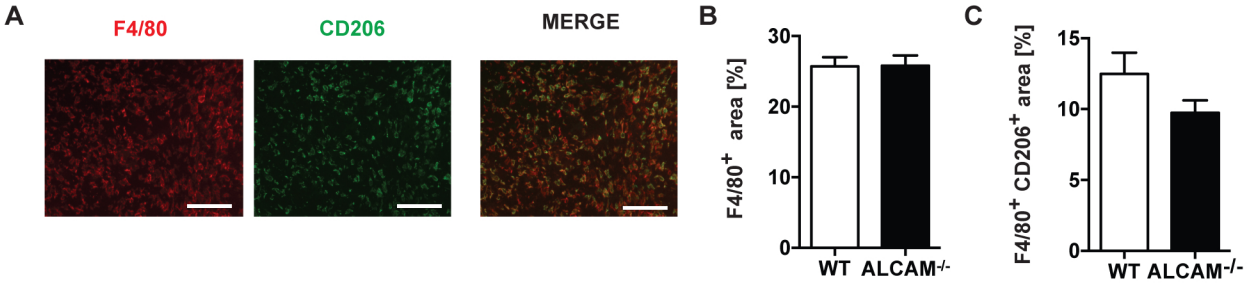

Supplemental Figure 3

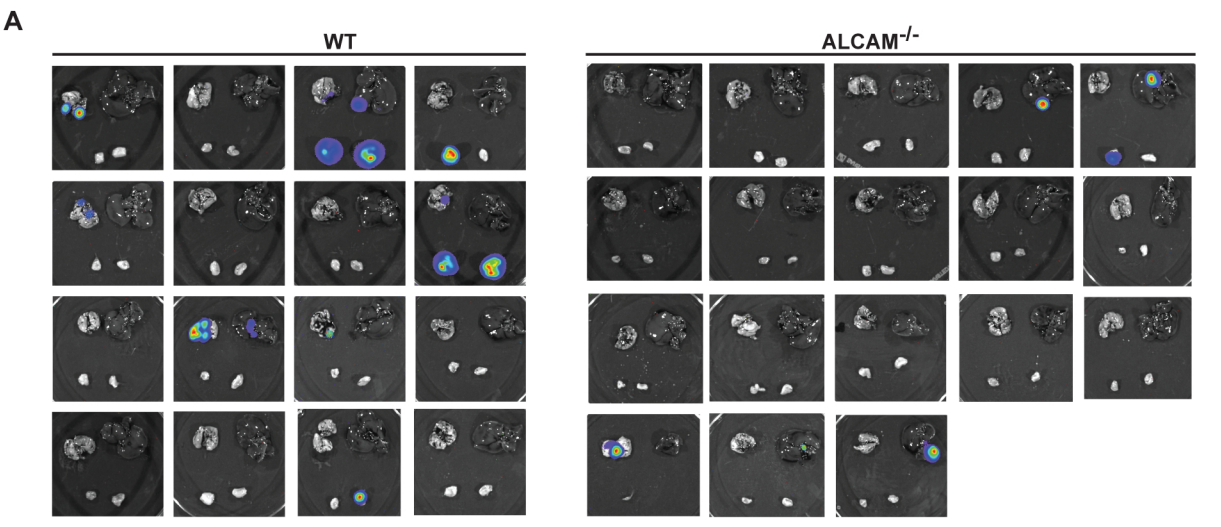

Supplemental Figure 4